

Focused Synthetic Radar Imaging Approach for Multi-tumor Screening

Abdullah Alqallaf* and Rabie Dib

**Department of Electrical Engineering, College of Engineering and Petroleum, Kuwait University, Kuwait*

Department of Electronics Engineering, College of Technological Studies, Public Authority of Applied Education and Training, Kuwait

**Corresponding Author: al.qallaf@ku.edu.kw*

ABSTRACT

In the last two decades, microwave imaging methods for early detection of possible tumors has received ample amount of attentions. As a non-ionizing radiator, the microwave imaging has a definite advantage over X-ray mammography, which is currently the main method of breast cancer diagnosis. This paper presents a focused synthetic radar imaging approach to detect the possible existing tumors and to clearly identify their sizes and locations to assist the physicians in cancer prognosis. Both analytical and simulation results are obtained for assumed tumors of different sizes and locations. This is done by modeling the breast tissues and the design of illuminating antenna. Comparing the detection performance with the conventional methods, the proposed approach outperforms the digital X-ray mammograms with sensitivity of 93.8% and specificity of 95.2%. Finally, the proposed study includes the required design elements of the optimized antenna used for accurately locating the tumors within a minimal margin of error.

Keywords: Synthetic Radar Imaging, Multi-Tumors Detection, Focusing Antenna.

INTRODUCTION

Breast cancer is a complicated disease with a variety of different causes. According to the International Agency for Research on Cancer (IARC), the Geneva Cancer Registry database, the European Network of Cancer Registries, and recent studies, breast cancer incidence among women under the age of forty has increased dramatically over years according to the International Agency for Research on Cancer (IARC 2012). Among Kuwaiti population, the breast cancer for females had the highest incidence and it had increased by 3-fold (50 cases /100,000 populations) over the last 33 years (Elbasmi et al., 2010). Although more patients are surviving due to early screening tests, breast cancer is the most common cancer worldwide and it has been on the rise for several years. While male breast cancer is rare, it occurs in both men and women. The estimated new cases are 226,870 females to 2,190 males and the deaths from breast cancers are 39,510 females to 410 males in the United States in 2012 according to the National Cancer Institute (NCI). Early screening tests and examinations for breast cancer are vital to find the disease before it starts to cause symptoms. The X-ray mammography has been proposed as the most approved method of breast imaging. However, it has basic limitations due to the small contrast between the diseased and normal tissue at the X-ray frequencies (Jackson et al., 1993, Brown et al., 1995, Huynh et al., 1998, Elmore et al., 1998). During imaging, the breast is compressed in order to create uniformity, in an otherwise heterogeneous tissue, and to avoid image blurring. This compression causes pain or at least discomfort that may reduce the patient compliance to safety recommendations. Microwave detection of cancerous tumors has been of great interest as an alternative or a complementary method to ionizing radiation methods such as computed tomography or mammography. Furthermore, microwave imaging enjoys the advantage of a clear contrast between the healthy tissues and diseased tissues or tumors (Chaudhary et al., 1984, Surowiec et al., 1988, Joines et al., 1994, Hagness et al., 2000). While the relative permittivity of normal tissues is around 10, that of the tumor is 50. There is also contrast between the conductivities, being about 0.15 S/m for normal tissue and 0.7 S/m for tumors. Recently, growing efforts appear in the literature for verifying the possibility of microwave imaging of the breast. Two approaches can be identified: the tomographic method that involves inverse

scattering technique (Souvorov et al., 1998) and the confocal imaging that is based on the concept of synthetic radar imaging (Hagness et al., 1999, Li and Hagness, 2001). The tomographic method uses the backscattered waves in an algorithm to reconstruct an image of the breast, in terms of tissue electrical parameters. The problem is considered an ill-conditioned nonlinear one and normally requires intensive computational work (Caorsi et al., 1993, Souvorov et al., 1998, Chew et al., 1998, Franchois et al., 1998, Bertero et al., 2000). This is so due to the heterogeneous nature of the breast medium. However some initial successful experimental results appear in Meaney et al. (1999, 2000). The method of confocal microwave imaging is based on the concept of synthetic radar imaging where the antenna focuses waves on small volume within the breast. This volume is scanned to provide an image of the whole breast volume as studied by Hagness et al., 1999, Li and Hagness, 2001. Further studies (Fear et al., 1999, 2000, 2002) confirm the method by simulation and experiment. They also show the robustness of the method to variations of the dielectric properties of the breast tissues. Such variations cause clutter in the received response that can be reduced by the power of focusing. An attempt for further reduction of such clutter is described recently by Byrne et al. (2010) who use a rotating antenna array. Two positions for the breast are used during imaging: the supine position and the prone position (Hagness et al., 1998, Fear et al., 1999, 2000, 2002). In the supine position the breast is oriented upwards and flattened out. A broadband antenna is placed on top and is fed by a suitable pulse. The return pulse is recorded and the early time response is cancelled as it comes from the skin layer. The response is taken at different antenna positions. Signal processing is then used, as in synthetic aperture radar for constructing an image. In the prone position, on the other hand, the breast is oriented downwards and therefore it resembles a cylinder. Again an antenna is placed on the cylindrical surface to send a broadband pulse (5.4 GHz – 5.9 GHz). The return pulses for different antenna positions are used to image the breast. Figure 1 is a graphical representation of the human breast structure, antenna orientations, and the breast tumors with different sizes and locations.

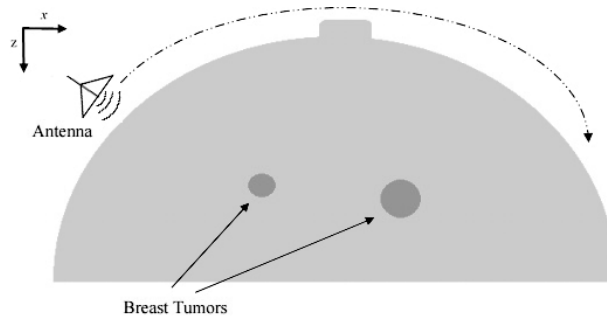


Fig. 1. Illustration of the human breast structure. The dashed curve represents the designed antenna path and the orange dots represent the breast tumors.

In this paper, we apply a focused synthetic radar imaging approach for the detection of the possible existing tumors. This is to assist the physicians in cancer prognosis to clearly map and detect the tumors locations and their sizes. The compact antenna used here is based on optimizing our previously designed antenna (Alqallaf et al., 2016). It shows that the optimum frequencies for detecting tumors depend on the tumors' radii and it is recommended that images should be taken at few distinct frequencies in the range 5-7 GHz in order to detect tumors of different sizes.

OPTIMIZED ANTENNA DESIGN AND EXPERIMENTAL MODELING

In general, there are two possible positions for the breast that can be used during the imaging process, the supine position and the prone position. In the supine position the breast is oriented upwards and flattened out, while in the prone position the breast is oriented downwards (Hagness et al., 1998). Here, we consider breast imaging in the supine position. The breast is assumed as a homogeneous medium having complex dielectric constant with conductivity σ (S/m) and relative permittivity ϵ_r . The possible existing tumors are modeled as small spherical like shape inhomogeneous

geneity having contrast conductivity σ_s and relative permittivity ϵ_{rs} . The breast is then modeled as a rectangular box with upper surface coinciding with $Z=0$ plane with a width of to 200 mm and a depth of 150 mm. Possible tumors of spherical shape with different radii exist at a depth d , i.e., at $Z=-d$. Using Computer Simulation Technology (CST) Microwave Studio Suite, an antenna is placed with its phase center at the origin of (x,y,z) coordinate system and radiates in the breast medium. While the relative permittivity ϵ_r of normal tissues is around 10, that of the tumor is 50. There is also contrast between the conductivities, being about 0.15 S/m for normal tissue and 0.7 S/m for tumors (Hagness et al., 1998). Table 1 summarizes the conductivity and relative permittivity parameters of the human. The choice of a suitable antenna for breast cancer detection is very crucial matter. The antenna is required to be compact, wide band, low profile, light weight, and flexible enough to be placed directly on the breast.

Table 1. Summarization of the human tissues parameters of the breast and tumors.

Tissue	Conductivity σ (S/m)	Relative permittivity ϵ_r
Tumor	0.7	50
Breast	0.15	10

Several antenna designs have been proposed for breast tumor detection including the dielectric resonator antenna (Fear et al., 2000), the stacked patch antenna (Fear et al., 2002), the wide slot UWB antenna (Byrne et al., 2010), and the flexible bowtie (Huang and Kishk, 2007). All of these antennas meet the required traits of a breast tumor sensor. Table 1 illustrates the conductivity and relative permittivity parameters of the human breast healthy tissues and the tumors as described in Hagness et al. (1998). For this, a compact flexible bowtie antenna is used in this study as a detective probes handled by the operator. The optimized antenna geometry and dimensions are chosen as in Figure 2 and Table 2 to operate around the center frequency of 5.5 GHz. This frequency is chosen as a compromise between required depth of penetration in the tissues and the existing tumors locations with suitable resolution as described in Alqallaf et al. (2016). The metal body of the bow-tie is printed on two thin flexible dielectric sheets as suggested by Huang and Kishk (2007) and is fed by a microstrip line as shown in Figure 2. The total thickness of the two dielectric sheets equals 0.1287 mm. The dielectric sheet is 0.05 mm thick and has a relative permittivity of 4. A matching scheme is designed with the feed line as shown in Figure 2. The resulting reflection loss $|S_{11}|$, when the antenna is placed on a medium that resembles the breast electrical properties, is given in Figure 3. It is seen that a -10 dB reflection loss or more is secured in the frequency ranges 5.2-6 GHz.

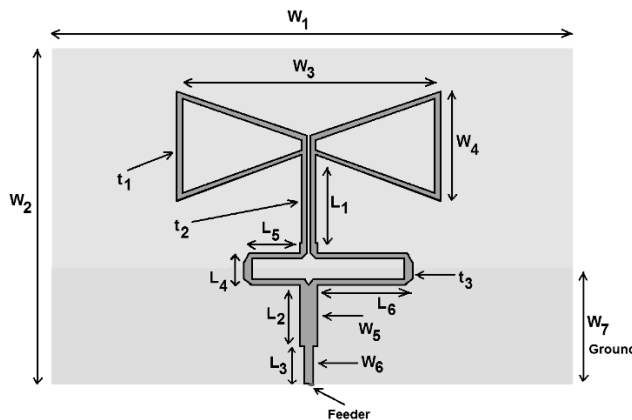


Fig. 2. Compact bow-tie antenna used for imaging. The optimized antenna dimensions are given in Table 2. The antenna is placed on a medium with the breast-like permittivity.

Table 2. Compact bow-tie antenna dimensions used for imaging.

Parameters	Length in (mm)
W ₁	30
W ₂	20
W ₃	15.6
W ₄	6.34
W ₅	0.48
W ₆	0.37
W ₇	6
L ₁	6.45
L ₂	3.44
L ₃	1.48
L ₄	1.18
L ₅	2.14
L ₆	5.92
t ₁	0.3
t ₂	0.28
t ₃	0.28

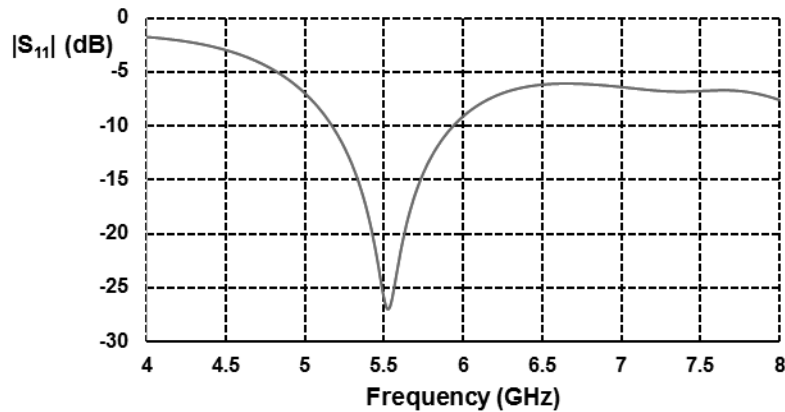


Fig. 3. The reflection of the compact bow-tie antenna $|S_{11}|$ in dB, y -axis, versus the frequency, in GHz, x -axis.

THEORETICAL ANALYSIS

To determine the scattered field from the inhomogeneity of the possible tumors, we assume that the diameters of the tumors are less than the applied wavelength. The incident wave is a single-plane wave focused from the antenna phase center at each position to the tumors centers in the radial coordinate r . With this assumption, the incident radial field can be determined from the sphere center in the form:

$$E_r^i = \frac{E_o \cos \phi}{jkr} \sum j^{-n} (2n + 1) \hat{j}_n(kr) \frac{\partial}{\partial \theta} P_n^{(1)}(\cos \theta) \tag{1}$$

here $k = \omega \sqrt{\mu_0 \epsilon_0 (\epsilon_r - \frac{j\sigma}{\omega \epsilon_0})}$ is the complex wave number and $\hat{j}_n(kr)$ is the spherical Bessel function and $P_n^{(1)}$

($\cos \theta$) is the associated Legendre polynomial. The incident radial field in (1) is also derivable from a magnetic vector potential A_r , so that $E_r^i = (j\omega\epsilon)^{-1} \left[\frac{\partial^2}{\partial r^2} + k^2 \right] A_r^i = (j\omega\epsilon)^{-1} \frac{n(n+1)}{r^2} A_r^i$.

Therefore,

$$A_r^i = \frac{E_o}{\omega\mu} \cos \phi \sum_{n=0}^{\infty} a_n J_n(kr) P_n^{(1)}(\cos \theta) \quad (2)$$

where $a_n = j^{-n}(2n+1)/(n(n+1))$. Similarly, for the radial magnetic field, the incident electric vector potential:

$$F_r^i = \frac{E_o}{k} \sin \phi \sum_{n=0}^{\infty} a_n J_n(kr) P_n^{(1)}(\cos \theta) \quad (3)$$

The scattered fields have similar form except that $\hat{j}_n(kr)$ is replaced by the spherical Hankel function $\hat{H}_n(kr)$. The total external field to the sphere is the sum of the incident and scattered fields, formally

$$\begin{aligned} A_r^{ex} &= \frac{E_o}{\omega\mu} \cos \phi \sum_{n=0}^{\infty} (a_n J_n(kr) + b_n \hat{H}_n(kr)) P_n^{(1)}(\cos \theta) \\ F_r^{ex} &= \frac{E_o}{k} \sin \phi \sum_{n=0}^{\infty} (a_n J_n(kr) + c_n \hat{H}_n(kr)) P_n^{(1)}(\cos \theta) \end{aligned} \quad (4)$$

where b_n and c_n are the scattered field coefficients. The internal fields inside the spherical tumor, namely,

$$\begin{aligned} A_r^{in} &= \frac{E_o}{\omega\mu} \cos \phi \sum_{n=1}^{\infty} d_n J_n(k_s r) P_n^{(1)}(\cos \theta) \\ F_r^{in} &= \frac{E_o}{k_s} \sin \phi \sum_{n=1}^{\infty} e_n J_n(k_s r) P_n^{(1)}(\cos \theta) \end{aligned} \quad (5)$$

where again d_n and e_n are the internal fields coefficients and $k_s = \omega \sqrt{\mu_0 \epsilon_0 (\epsilon_{rs} - \frac{j\sigma_s}{\omega \epsilon_0})}$ is the wave number in the spherical tumor.

Applying the boundary conditions to determine the unknown coefficients b_n and c_n requires the continuity of the θ and ϕ -field components at the spherical surface $r=a$. The scattered field external region component is

$$E_\theta^S(r, \theta) = \frac{-E_o}{kr} \cos \phi \sum_{n=1}^N c_n \hat{H}_n(kr) \frac{P_n'(cos\theta)}{\sin\theta} + j b_n \hat{H}_n'(kr) \frac{\partial P_n'(cos\theta)}{\partial \theta} \quad (6)$$

where b_n and c_n are obtained at $r=a$ as

$$b_n / a_n = [\bar{\eta}_s R_{ns} \hat{J}_n(ka) - \hat{J}_n'(ka)] / [\hat{H}_n'(ka) - \bar{\eta}_s R_{ns} \hat{H}_n(ka)] \quad (7)$$

$$c_n / a_n = [\bar{k}_s R_{ns} \hat{J}_n(ka) - \hat{J}_n'(ka)] / [\hat{H}_n'(ka) - \bar{k}_s R_{ns} \hat{H}_n(ka)] \quad (8)$$

here the prime on top of the Bessel and the Hankel spherical functions represents the differentiation with respect to the argument, $\bar{\eta}_s = \eta_s / \eta$, $\bar{k}_s = \frac{k_s}{k}$, and $R_{ns} = \hat{J}_n(k_s a) / \hat{H}_n(k_s a)$, where η is the wave impedance in the breast medium. The summation term is truncated after N terms, where N depends on the tumor size. Arithmetic calculations show that $N=5$ gives acceptable convergence up to tumor radius of 7 mm at 5.5 GHz applied frequency. The scattered field at the transmission is equal to $E_\theta(r_1, \pi) (-\frac{d}{r_1})$, where $r_1 = \sqrt{d^2 + L^2}$. Here, d and L are the vertical and the horizontal displacements between the focused antenna and the center of the tumor, respectively.

The next step is applying signal processing approach to realize focusing on the tumor for M locations of the antenna at $L = i\Delta; i=0, 1, 2 \dots (M-1)$. The total sum of the signals for the M locations of the antenna is

$$E_{total} = \sum_{i=0}^{M-1} [E_{\theta}(r_1, \pi) (-\frac{d}{r_1})] \exp[+2jkr_1] \quad (9)$$

The focused antenna is placed in 17 equi-spaced locations with an increment of $\Delta = 10$ mm. The field is normalized relative to the incident radial field, E . The response tends to increase with the tumor radius, but in an oscillatory manner as noted in Alqallaf et al. (2016). It was also shown that the theoretical and simulation results are in good agreement.

EXPERIMENTAL SETUP

A practical model to the reality has been developed for simulating the breast tissue and a parametric study has been performed in the presence of multiple tumors in the tissue in which we used the trajectory of movement of the focused antenna. The designed antenna has been optimized to minimize the operational error in detecting the possible tumors based on the finite element analysis of the scattering field of the incident wave radiated by a wideband dipole antenna and received by the same antenna positioned in a way that satisfies the requirements in the absence of obstacle which is a tumor of any size. As described in the previous section, the critical dimensions of the wideband antenna design have been studied parametrically within the finite element simulations to optimize the contrast of the scattering among the cases of different number of presented tumors. The optimized antenna will be the detective probes handled by the operator in the final fabrication stage of the design. The full three-dimensional solver for discrete number of frequency points has been employed to provide the radiation pattern variations in the design process. This accurately delivered the 3D electromagnetic simulations of the frequency using Computer Simulation Technology (CST) Microwave Studio Suite and MATLAB programming.

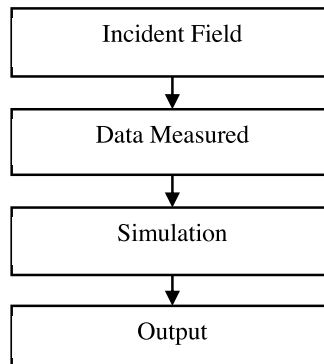


Fig. 4. General proposed process representation.

Figure 4. illustrates the general planned process of the experimental setup from the incident field until the image formation of tumors detection.

IMAGE RECONSTRUCTION ALGORITHM AND EVALUATION

Since the scattered signal is measured in frequency-domain, hence, a comprehensive signal processing algorithm, namely, the Inverse Fast Fourier Transform (IFFT), has been used to transform the signal to time-domain. The time-domain backscatter signals are analyzed and an artifact removal is being applied using data adaptive algorithm to remove (subtract) the early time artifacts at the received signals of tumors reflection. This is for clearly mapping and locating of the detected tumors and to generate the exact coordinates to be used in the radiotherapy treatments.

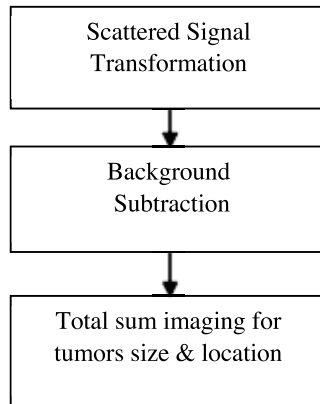


Fig. 5. Block diagram of the breast imaging reconstruction.

Figure 5. shows the process of image formation process. The measured data represent the scattered signal received from any position under consideration and the areas with tumors and without tumors are subtractions in order to obtain the tumor. Then, the total sum imaging is applied with the consideration of time delay to get the spatial focusing of the backscattered signals for image formation of tumors location.

SIMULATION RESULTS AND DISCUSSIONS

The antenna is placed on the breast surface and is fed by a pulse that covers a bandwidth of 500 MHz around 5.5 GHz center frequency. The pulse bandwidth is less than 10% of the center frequency. Within this narrow bandwidth, the breast electrical parameters can be assumed constants and therefore, one can accurately compensate for the propagation effects in the breast. One can apply the pulse at different discrete center frequencies to obtain multi-frequency images for the tumor. The voltage waveform picked up by the antenna is monitored for, say, M different positions of the antenna as it is displaced along the X -axis. To remove the primary pulse and possible reflections from the skin layer of the breast, the average received waveform from the M positions is subtracted from each of the received waveforms. The resulting signals represent the scattered field from the tumor inhomogeneity at the M antenna positions. The next step is to process the M signals so as to synthetically focus the field at an arbitrary point within the breast. This leads to imaging the breast medium. In processing the M waveforms, we have to account for the variations of the antenna radiation pattern at the scanned points. The response obtained from a spherical tumor of radius 6 mm in the X - Z plane is shown is Figure 6.

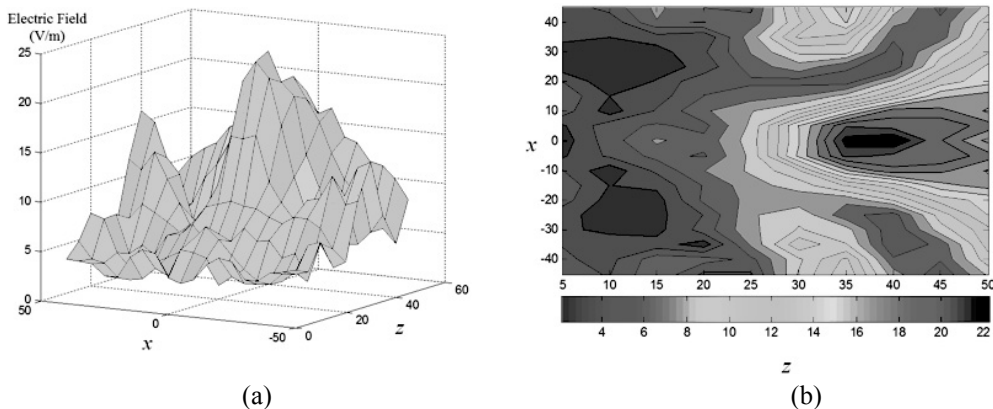


Fig. 6. Reflection response versus observing point on the x - z plane for 6mm radius tumor. a) 3-dimensional plot. b) Contours of constant reflection.

The breast is modeled as a block of width 200 mm, and depth of 100 mm. The response in Figure 6a is obtained for $M=17$ positions of the antenna on the $Z=0$ plane. The contours of constant response levels are shown in Figure 6b. The obtained results in Figure 6 show an agreement between the peak and tumor location with few millimeters shift. Figures 7a,b show the same response as in Figures 6a,b, except that multi-tumors are suggested. It is clear from both figures that there is a clear peak response at the exact position and a little shifted depth of the tumor. The resolution may be determined by the region where the response is reduced to 50% of the peak value. For the single tumor of 6mm, the resolution region covers 20 mm about the X position and about 15 mm in the Z -direction. This means that two tumors separated horizontally by less than 20 mm or vertically by 15 mm cannot be distinguished and will be shown as one tumor. It is interesting to study the reflection level as a function of the tumor radius at a given depth.

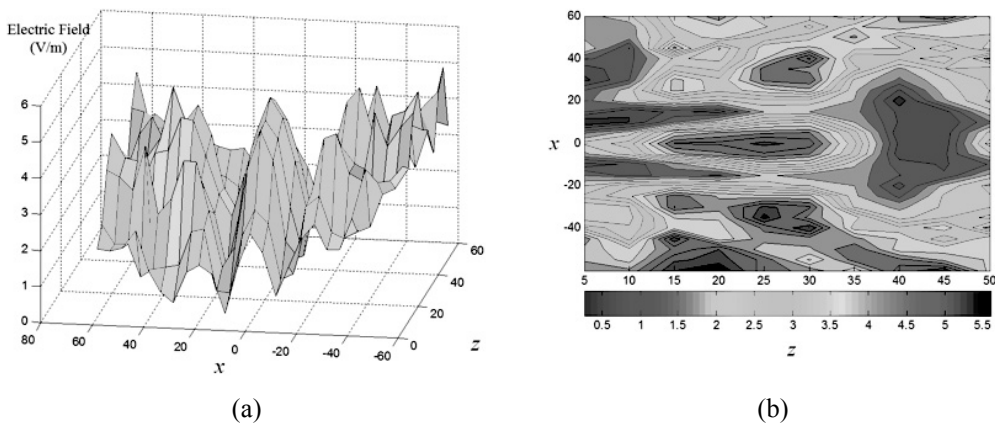


Fig. 7. Reflection response versus observing point on the x - z plane for 6mm radii tumors. a) 3-dimensional plot. b) Contours of constant reflection.

Figure 8 presents the result of two tumors with different radii (one is double the other in size), and the figure shows two peaks with different values at almost the same location of the tumors.

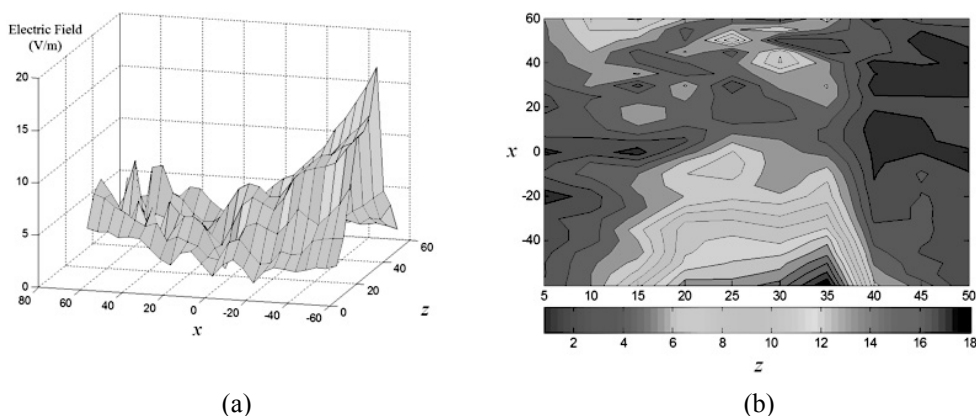


Fig. 8. Reflection response versus observing point on the x - z plane for 4mm and 8mm radii tumors. a) 3-dimensional plot. b) Contours of constant reflection.

In this study, we demonstrate the capability to detect and localize small (<4 mm) tumors within the breast phantom. As demonstrated in Table 3, the detection performance capabilities of the proposed method for detecting primary breast tumors based on the sensitivity and the specificity of 93.8% and 95.2%, respectively, is compared to the conventional approaches, the digital X-ray mammograms (Kerlikowske et al., 2011), of 82.4% and 89.7%, respectively.

Table 3. Detection performance measurements for detecting primary breast tumors.

Parameter	Proposed approach	Digital Mammograms
Sensitivity	93.8%	82.4%
Specificity	95.2%	89.7%

CONCLUSION

In this paper, we present a focused synthetic radar imaging approach for breast cancer screening using an optimized antenna. The proposed method provides a low-risk tool, non-ionized radiation, for the detection of multiple tumors simultaneously. This is done by modeling the breast as a homogeneous medium, while the tumors are modeled as small spherical inhomogeneity. To clearly map and locate the possible existing tumors, the proposed approach is applied using compact antenna. It is demonstrated that the spherical-like tumor can be detected with reasonable resolution using a narrow band pulse of 5.5 GHz center frequency and 0.5 GHz bandwidth. The simulation results are supported by analytical results where a reasonably good agreement is observed. Finally, the simulation results provide an evidence of detecting the possible existing tumors as small as small (<4 mm) at early stages with a minimal marginal error of a radius of at most 0.5cm from their original locations within the breast phantom.

ACKNOWLEDGMENT

This work was supported by Kuwait University Research Grant No. [EE03/16].

REFERENCES

- Alqallaf, A. K., Dib, R. K. & Mahmoud, S. F. 2016. Microwave Imaging Using Synthetic Radar Scheme Processing for the Detection of Breast Tumors: The Applied Computational Electromagnetics Society, 31: 98-105.
- Brown, M., Houn, F., Sickles, E. & Kessler, L. 1995. Screening mammography in community practice: Amer. J. Roentgen., 165: 1373-1377.
- Huynh, P. T., Jarolimek, A. M. & Daye, S. 1998. The false-negative mammogram: Radiograph., 18: 1137-1154.
- Elmore, J. G., Barton, M. B., Mocerri, V. M., Polk, S., Arena, P. J. & Fletcher, S. W. 1998. Ten-year risk of false positive screening mammograms and clinical breast examinations: New Eng. J. Med., 338: 1089-1096.
- Jackson, V. P., Hendrick, R. E., Feig, S. A. & Kopans, D. B. 1993. Imaging of the radiographically dense breast: Radiology, 188: 297-301.
- Surowiec, A. J., Stuchly, S. S., Barr, J. R. & Swarup, A. 1988. Dielectric properties of breast carcinoma and the surrounding tissues: IEEE Trans. Biomed. Eng., 35: 257-263.
- Joines, W. T., Zhang, Y., Li, C. & Jirtle, R. L. 1994. The measured electrical properties of normal and malignant human tissues from 50 to 900 MHz: Med. Phys., 21: 547-550.
- Chaudhary, S. S., Mishra, R. K., Swarup, A. & Thomas, J. M. 1984. Dielectric properties of normal and malignant human breast tissues at radiowave and microwave frequencies: Indian J. Biochem. Biophys., 21: 76-79.
- Hagness, S. C., Leininger, K. M., Booske, J. H. & Okoniewski, M. 2000. Dielectric characterization of human breast tissue at microwave frequencies: presented at the 2nd World Congr. Microwave and Radio Frequency Processing.
- Caorsi, S., Gragnani, G. L. & Pastorino, M. P. 1993. Reconstruction of dielectric permittivity distributions in arbitrary 2-D inhomogeneous biological bodies by a multiview microwave numerical method: IEEE Trans. Med. Imag., 12: 232-239.
- Souvorov, A. E., Bulyshev, A. E., Semenov, S. Y., Svenson, R. H., Nazarov, A. G., Sizov, Y. E. & Tatsis, G. P. 1998. Microwave tomography, A two-dimensional Newton iterative scheme: IEEE Trans. Microwave Theory Tech . , 46: 1654-1659.
- Chew, W. C. 1998. Advances in Computational Electrodynamics: The Finite-Difference Time-Domain Method, A. Taflove, Ed. Norwood, MA: Artech House, ch. 12.

- Franchois, A., Joisel, A., Pichot, C. & Bolomey, J. C. 1998.** Quantitative microwave imaging with a 2.45-GHz planar microwave camera: *IEEE Trans. Med. Imag.*, 17: 550-561.
- Bertero, M., Miyakawa, M., Boccacci, P., Conte, F., Orikasa, K. & Furutani, M. 2000.** Image restoration in chirp-pulse microwave CT (CP-MCT): *IEEE Trans. Biomed. Eng.*, 47: 690-699.
- Meaney, P. M., Paulsen, K. D., Chang, J. T., Fanning, M. W. & Hartov, A. 1999.** Nonactive antenna compensation for fixed-array microwave imaging—Part II: Imaging results: *IEEE Trans. Med. Imag.*, 18: 508-518.
- Meaney, P. M., Fanning, M. W., Li, D., Poplack, S. P. & Paulsen, K. D. 2000.** A clinical prototype for active microwave imaging of the breast: *IEEE Trans. Microwave Theory Tech.*, 48:1841-1853.
- Hagness, S. C., Taflove, A. & Bridges, J. E. 1998.** Two-dimensional FDTD analysis of a pulsed microwave confocal system for breast cancer detection: fixed-focus and antenna-array sensors: *IEEE Trans. Biomed. Eng.*, (45) 1470-1479.
- Hagness, S. C., Taflove, A. & Bridges, J. E. 1997.** Wideband ultra low reverberation antenna for biological sensing: *Electron. Lett.*, 33(19): 1594-1595.
- Hagness, S. C., Taflove, A. & Bridges, J. E. 1999.** Three-dimensional FDTD analysis of a pulsed microwave confocal system for breast cancer detection: design of an antenna-array element: *IEEE Trans. Antennas Propagat.*, (47) 783-791.
- Li, X. & Hagness, S. C. 2001.** A confocal microwave imaging algorithm for breast cancer detection: *IEEE Microwave Wireless Comp. Lett.*, 11: 130-132.
- Fear, E. C. & Stuchly, M. A. 1999.** Microwave system for breast tumor detection,” *IEEE Microwave Guided Wave Lett.*, 9: 470-472.
- Fear, E. C. & Stuchly, M. A. 2000.** Microwave detection of breast cancer: *IEEE Trans. Microwave Theory Tech.*, 48: 1854-1863.
- Fear, E. C. & Stuchly, M. A. 2000.** Microwave detection of breast tumors: Comparison of skin subtraction algorithms,” *Proc. SPIE*, 41(29) 207-217.
- Fear, E. C., Li, X., Hagness, S. C. & Stuchly, M. A. 2002.** Confocal Microwave Imaging for Breast Cancer Detection: Localization of Tumors in Three Dimensions: *IEEE TRANSACTIONS ON BIOMEDICAL ENGINEERING*, 49 (8).
- Byrne, D., O’Halloran, M., Jones, E. & Glavin, M. 2010.** Transmitter-grouping robust capon beamforming for breast cancer detection: *Progress In Electromagnetics Research*, 108: 401-416.
- Huang, W. & Kishk, A. 2007.** Compact wideband multi-layer cylindrical dielectric resonator antennas: *IEE Proc. Microw. Antennas Propag.*, 1(4): 998-1005.
- Huang, W. & Kishk, A. 2009.** Compact dielectric resonator antenna for microwave breast cancer detection,” *IET Microwave, Antennas & propagation*, 3(4): 638-644.
- Nilavalan, R., Craddock, I. J., Preece1, A., Leendertz1, J. & Benjamin, R. 2007.** Wideband microstrip patch antenna design for breast cancer detection: *IET Microw. Propag.*, 1(2): 277-281.
- Gibbins, D., Klemm, M., Craddock, I. J., Leendertz, J. A., Preece, A. & Benjamin, R. 2010.** A comparison of a wide-slot and a stacked patch antenna for the purpose of breast cancer detection: *IEEE Transactions on Antennas and Propagation*, 58(3): 665-674.
- Durgun, A. C., Balanis, C. A., Birtcher, C. R. & Allee, D. A. 2011.** Design, Simulation, Fabrication and Testing of Flexible Bow-Tie Antennas: *IEEE Transactions on Antennas and Propagation*, 59(12).
- Abramowitz, M. & Stegun, I. A. Ed., 1970.** *Handbook of Mathematical Functions*: Chap. 10 by H. Antosiewicz, Dover Publications. Inc., New York.
- Harrington, R. F. 1961.** *Time Harmonic Electromagnetic Fields*: Chapter 6, McGraw Hill.
- Eldek, A. A., Elsherbeni, A. Z. & Smith, C. E. 2005.** Wideband Modified Printed Bow-Tie Antenna with Single and Dual Polarization for C and X-Band Applications,” *IEEE Transaction on Antennas and Propagations*, 53 (9): 3067-3072.
- Porter1, E., Walls, G., Zhou, Y., Popovic, M. & Schwartz, J. D. 2014.** A Flexible Broadband Antenna and Transmission Line Network for a Wearable Microwave Breast Cancer Detection System: *Progress In Electromagnetics Research Letters*, 49:111-118.

- Wang, Z., Lim, E. G., Tang, Y. & Leach, M. 2014.** Medical Applications of Microwave Imaging: The Scientific World Journal, 2014.
- Singh, P. K., Tripathi, S. K., Sharma, R. & Kumar, A. 2013.** Design & Simulation of Microstrip Antenna for Cancer Diagnosis: International Journal of Scientific & Engineering Research, 4(11): 1821-1824.
- Brown, M., Houn, F., Sickles, E. & Kessler, L. 1995.** Screening mammography in community practice: Amer. J. Roentgen., 165: 1373-1377.
- International Agency for Research on Cancer (IARC) and World Health Organization (WHO) 2012.** GLOBOCAN: Estimated cancer incidence, mortality and prevalence worldwide.
- Kerlikowske K., Hubbard R., Miglioretti D., Geller B., Yankaskas B., Lehman C., Taplin S. & Sickles E. 2011.** Comparative effectiveness of digital versus film-screen mammography in community practice in the United States: a cohort study. Annals of Internal Medicine 155(8): 493-502.
- Elbasmfi, A., Al-Asfour, A., Al-Nesf, Y. & Al-Awadi A. 2010.** Cancer in Kuwait, magnitude of the problem: Gulf J Oncolog., 8: 7-14.

Submitted: 03/08/2017

Revised: 26/11/2017

Accepted: 29/11/2017

النهج الراداري المركز للكشف عن الأورام المتعددة

*عبدالله القلاف وربيع ديب

*قسم الهندسة الكهربائية، كلية الهندسة والبتترول، جامعه الكويت، دولة الكويت
قسم الهندسة الالكترونية، كلية الدراسات التكنولوجية، الهيئة العامة للتعليم التطبيقي والتدريب، دولة الكويت

الخلاصة

في العقدين الماضيين، تلقت طرق التصوير بالموجات الدقيقة للكشف المبكر عن الأورام المحتملة وفرصة من الانتباه. وباعتباره طريقة بديلة غير مؤينة، فإن التصوير بالميكروويف له ميزة واضحة على التصوير الشعاعي للثدي بالأشعة السينية والذي هو حالياً الطريقة الرئيسية لتشخيص سرطان الثدي. يعرض هذا البحث نهج التصوير الراداري الاصطناعي المركز للكشف عن الأورام الموجودة الممكنة وتحديد أحجامها ومواقعها بوضوح لمساعدة الأطباء في تشخيص السرطان. تم الحصول على كل من النتائج التحليلية والمحاكاة للأورام المفترضة من مختلف الأحجام والمواقع. وتم ذلك عن طريق نمذجة أنسجة الثدي وتصميم هوائي مضيق. وأخيراً، تتضمن الدراسة المقترحة عناصر التصميم المطلوبة للهوائي الأمثل المستخدم لتحديد موقع الأورام بدقة ضمن هامش خطأ ضئيل.